First Measurement of the Spectral Function at High Energy and Momentum

D. Rohe*

University of Basel, CH–4056 Basel, Switzerland

Abstract. The experiment E97-006 was performed at Jefferson Lab to measure the momentum and energy distribution of protons in the nucleus far from the region of the (approximate) validity of the mean field description, i.e. at high momenta and energies. The occurrence of this strength has long been infered from occupation numbers less than one. In the experiment reported here this strength was directly measured for the first time. The distortion of the spectral function, due to secondary reactions of the knock-out nucleon when passing through the nucleus, is small for parallel kinematics. The results are compared to modern many-body theories. Further the transparency factor of ^{12}C was determined in the Q^2-region of 0.6 to 1.8 (GeV/c)^2.

1 Introduction

The energy and momentum distribution of nucleons bound in the nucleus are obviously determined by the nucleon-nucleon potential. The N-N potential consists of a repulsive core at small nucleon-nucleon distances of less than $\approx$ 1 fm and an attractive part. Realistic potentials are usually constructed based on N-N scattering data. In a vector meson exchange model the long-range part is represented by an exchange of a virtual pion whereas the short-range part is provided by heavier mesons like the omega and the rho (s. also contribution from R. Machleidt). The strongly repulsive part, which is caused by the short-range and tensor components of the interaction, is ignored in the mean field description (IPSM) where it is assumed that the nucleons move independently from each other. Therefore all nucleons reside below the Fermi energy and Fermi momentum of about 250 MeV/c. It came as somewhat of a surprise when (e,e$'$p) measurements, performed mainly at NIKHEF [1], found values of typically 65 % for the spectroscopic factor of the valence orbits in nuclei from lithium to lead. Short-range (SRC) and tensor correlations are responsible for up to 15 % depletion. Due to the repulsive core of the interaction at small distances nucleons are scattered to high energy and momentum. Another 20 % is coming from long-range correlations (LRC) which lead to a fragmentation of the single-particle states due to coupling to collective modes like vibrations. This influences the spectral function in particular at small energy, *i.e.* the valence states. For the deeper lying orbits the occupation is larger.

Modern many-body theories like the Correlated Basis Function theory (CBF) [2], the Green's function approach (GF) [3] and the self-consistent Green's function

* Present address: Paul Scherrer Institut, Villigen, Switzerland

theory (SCGF) [4] are able to deal with the realistic N-N potential directly and therefore contain short-range and tensor correlations. The remarkable difference to the momentum and energy distribution derived in the IPSM is the additional strength found at large energy E and momentum k. Above the Fermi momentum k_F the single-particle strength is negligible. As a consequence the search for SRC has to concentrate on large E and k. A practical tool is the (e,e′p) reaction.

2 Experiment

The experiment was performed in Hall C at Jefferson Lab employing three quasi-parallel and two perpendicular kinematics at a momentum transfer $q \gtrsim 1$ (GeV/c) (for a detailed discussion see [5]). Electrons of 3.3 GeV energy with beam currents up to 60 μA were incident upon ^{12}C, ^{27}Al, ^{56}Fe and ^{197}Au targets. The scattered electrons were detected in the HMS spectrometer (central momenta 2–2.8 GeV/c), the protons were detected in the SOS spectrometer (central momenta 0.8–1.7 GeV/c). Missing momenta of up to 650 MeV/c were explored.

From the measured scattering angles and momenta of the electron and the proton the missing energy

$$E_m = E_e - E_{e'} - T_{p'} - T_{A-1} \tag{1}$$

and the missing momentum

$$\vec{p}_m = \vec{q} - \vec{p}_{p'} \tag{2}$$

can be constructed. Here E_e is the electron beam energy, $E_{e'}$ the energy of the scattered electron and $T_{p'}$ (T_{A-1}) the kinetic energy of the knocked-out proton (the residual nucleus). In Plane Wave Impulse Approximation (PWIA) there is a direct relation between the measured quantities and the theory. In this case E_m can be identified with the removal energy E of the proton in the nucleus and p_m with its initial momentum $-\vec{k}$. However, in the nucleus the hit proton can interact with the other nucleons of the nucleus. Obviously this rescattering contribution is reduced for large momentum transfer q and increases for heavier nuclei. Calculations of the rescattering contribution [7] confirm that rescattering is small for ^{12}C in parallel kinematics where the momentum transfer $\vec{q}$ is parallel to the initial momentum of the proton (s. sec. 4). The data taken in perpendicular kinematics lead to a three times larger strength integrated over the experimental acceptance and compared to the parallel kinematics. Rescattering contributions alone cannot entirely explain this difference; MEC would need to be included.

In PWIA the spectral function can be obtained via the absolute differential cross section

$$\frac{d\sigma}{d\Omega_e\, d\Omega_p\, dE_{e'}\, dE_{p'}} = K\, \sigma_{ep}\, S(E_m, \vec{p_m})\, T_A(Q^2). \tag{3}$$

Here K is a kinematical factor and σ_{ep} the e-p cross section for a moving proton bound in the nucleus. Since the bound proton is off-shell, *i.e.* the usual relation between mass, energy and momentum is not longer valid, the expression for the e-p

cross section cannot be derived uniquely. Different versions are on the market like σ_{cc1} and σ_{cc2} [8] which are derived from two expressions of the electromagnetic current operator Γ_1 and Γ_2. Both are equivalent in the on-shell case but differ for an off-shell proton. In the following the e-p cross section σ_{cc} [5] will be used where the kinematical variables are not modified to obtain an equivalent on-shell kinematics as in the case of σ_{cc1} and σ_{cc2}. The difference between the cross sections is small in the IPSM region but increases with increasing p_m and E_m. The choice of σ_{cc} is motivated by the fact that it gives the best agreement of the spectral function for same E_m and p_m measured in different (parallel) kinematics.

The attenuation of the proton flux due to the N-N interaction in the nucleus is accounted for by the nuclear transparency T_A. T_A was measured for five different kinematics on ^{12}C which serves also for a check of the analysis procedure. The results are presented in the next section and compared to the correlated Glauber theory of Benhar [9]. Two-step scattering processes of the proton traversing the nucleus as well as π production distort the spectral function and are calculated in a semiclassical model [7, 10] (see Section 4).

3 Transparency

Measurements of the transparency rely on comparison of the yield measured N^{exp} for a specific nucleus to the yield N^{sim} calculated assuming PWIA.

$$T_A(Q^2) = \frac{\int_V d\mathbf{p}_m \, dE_m \, N^{exp}(E_m, \mathbf{p}_m)}{\int_V d\mathbf{p}_m \, dE_m \, N^{sim}(E_m, \mathbf{p}_m)}. \tag{4}$$

This transparency accounts for absorption of the proton in the nucleus but also for large momentum changes due to an interaction with the surrounding nucleons. The simulated yield accounts for the detector acceptances, radiative corrections etc. It is checked that the spectra from the simulation are in good agreement with the one measured or reconstructed from measured quantities. As input for the simulation a spectral function is needed. Because the spectral function is best known at small E_m and p_m, one restricts this measurement to the IPSM region. As boundaries $E_m <$ 80 MeV and $p_m < 300$ MeV/c are chosen, the same as used in previous analyses at SLAC and Jlab [11–13].

In the simulation a spectral function has to be chosen which should correctly describes the experimental distribution in the region of interest. In the previous analyses an IPSM spectral function was used which factorizes into E and k-dependent distributions. The E-distribution is described by a Lorentzian and the momentum distribution is derived from a Wood-Saxon potential whose parameters are adjusted to data measured at Saclay [16]. This spectral function does not account for any depletion of the shells due to N-N correlations. To take this into account the simulated yield for carbon is divided by a factor ϵ^{SRC} = 1.11 $\pm$ 0.03. This factor was used in all the previous analyses and was estimated from an early examination of N-N correlations in ^{12}C and ^{16}O [17, 18]. The inverse of ϵ^{SRC} corresponds to the

occupation number, which modern many-body theories predict to be lower, ≈ 80 - 85% [2,3]. This number is larger than the spectroscopic factor giving the occupation of a state; it contains the background strength, also caused by correlations, which cannot be attributed to a specific orbit [19, 20]. The above considerations emphasize that the number of nucleons missing due to absorption in the nucleus cannot be distinguished from the depletion of the single-particle orbits due to SRC.

The factor ϵ^{SRC} introduced in the IPSM spectral function to account for the depletion due to N-N correlations is certainly an approximation. Comparison to data for higher p_m (but still smaller than 300 MeV/c) reveal that the IPSM spectral function is already missing strength at $E_m > 0.05$ GeV. To improve upon this approach a spectral function containing SRC from the beginning is employed in Eq.(4). This spectral function is composed of a part due to SRC which accounts for 22% of the total strength as calculated in Local Density Approximation (LDA), and the IPSM spectral function mentioned above but reduced by a factor (1 – 0.22) to ensure normalization. This approach circumvents the application of the extra factor ϵ^{SRC}. In addition, much better agreement between measured and simulated E_m spectra is achieved. Using this spectral function the five data points for the nuclear transparency of ^{12}C (solid symbols) are obtained which are shown as a function of the proton kinetic energy in Figure 1 together with previous results obtained at SLAC [11] (circles) and Jlab [12, 13] (squares and diamonds). The error bars shown in the figure contain the statistical and systematic uncertainty but not the model-dependent error of 4.7 %. This applies also to the data points of the previous works. Since the previous experiments were analyzed using the same assumption and ingre-

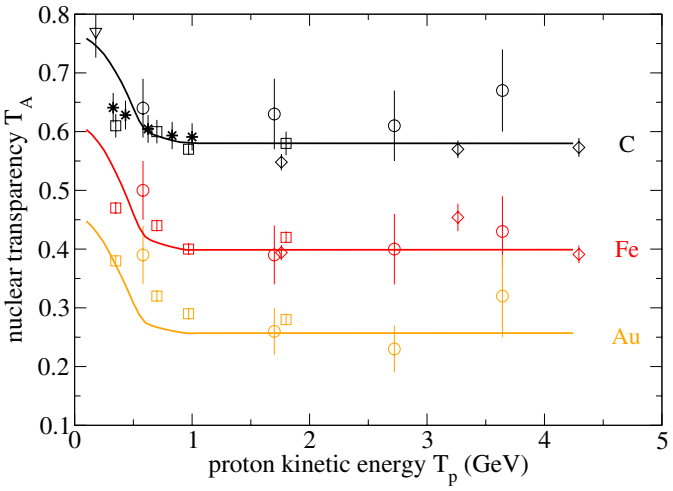

Figure **1.** Nuclear transparency T_A for C, Fe and Au as a function of the proton kinetic energy T_p compared to the correlated Glauber calculations (solid lines). Circles: NE18–experiment at SLAC [11]; squares, diamonds: Jlab [12], [13]; triangles down: Bates [14]. The result indicated by stars is obtained with the correlated spectral function of [15].

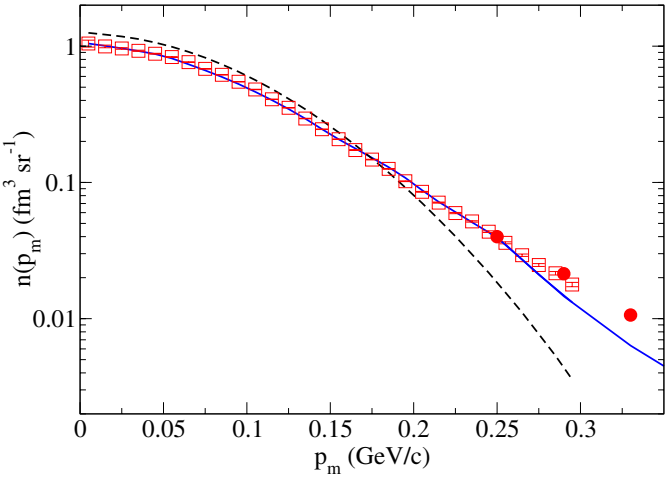

Figure **2.** Momentum distribution in the region of 0.03 GeV $< E_m <$ 0.08 GeV obtained from the data, the CBF theory (solid) and the IPSM (dashed). Three data points (circles) are from data focusing on the high p_m region [5, 21] (s. sec. 5).

dients the model-dependent error is the same for them, while it is somewhat lower in our case since we use the CBF spectral function.

The solid lines drawn in Figure 1 are the result of the correlated Glauber theory [9] which takes Pauli blocking, dispersion effects and N-N correlations into account. For comparison also results from previous experiments [11–13] for iron and gold are shown. For all three nuclei and large proton kinetic energy ($>$ 1.5 GeV) the theory describes the data well within the error bars. At low energy there is remarkable agreement between theory and the experimental results obtained using the CBF spectral function.

In Figure 2 the momentum distribution, mainly covering the $S_{1/2}$ state in ^{12}C (E_m= 0.03 - 0.08 GeV) is shown for the data (squares), the CBF theory and the IPSM. Obviously the IPSM momentum distribution starts to fail above $p_m \approx 200$ MeV/c. It exceeds the data for small p_m by about 20 % because no correction for SRC is applied. The CBF theory combined with the spectral function from IPSM as described above is in good agreement with the data. No extra renormalization factor is needed.

4 Calculation of the Contribution from Rescattering and Pion Production

The 2-step rescattering contribution was studied in a semiclassical model which has the advantage of describing the distortion due to FSI in terms of the full one-hole spectral function. This accounts for both the momentum and the energy distribution of the original correlated strength which is important for the proper description of

the response. In the model the primary (e,e′N) reaction (N = nucleon) is followed by a second N-N interaction in the nucleus with the condition that a proton is emitted within the acceptance of the spectrometer. The first reaction is described by PWIA similar to Eq. 3 except that the transparency factor is replaced by the transmission probability of a nucleon in medium. This factor gives the probability that the struck particle propagates without any interaction to a second point where it scatters from a second nucleon. The probablilty to find a second nucleon at a certain point is accounted for by the pair distribution function. For the second reaction the in-medium cross section is taken. The complete expression is integrated over the kinetic energy of the intermediate nucleon to obtain the cross section. For this calculation a spectral function as input is needed. At low energy and momenta the correlated part was taken from the spectral function calculated in CBF theory [2] combined with a properly scaled spectral function derived from a Wood-Saxon potential. For ^{12}C this part could be qualitatively compared with the data taken for extracting the transparency factor (see Section 3). At higher energy and momentum, where production data in parallel kinematics are available, the experimental distorted spectral function was fitted with a Lorentzian distribution and an exponential tail. The increase of the spectral function in the resonance region was ignored.

The second contribution to the (e,e′p) cross section comes from the production of an undetected pion. The mass and the energy carried by the pion will appear in the kinematical reconstruction as additional missing energy. Therefore the bump appears at higher E_m and is well separated. The cross section was obtained in the PWIA approach using the response function for pion production from the MAID program. The response function depends on the invariant mass and the angle between pion and proton in the c.m. frame.

From these two cross sections a distorted spectral function is obtained according to Eq. 3. It is compared to the experimental result in Figure 3 for four p_m bins. The effect of rescattering is quite small in parallel kinematics. This is expected from kinematical considerations. Due to rescattering the emitted nucleon loses part of its energy by knocking out a second particle. The condition of small angles between the momenta p_i (initial momentum) and q implies larger kinetic energies (i.e. small E_m) and larger p_m for the intermediate nucleon with respect to the detected nucleon. Therefore the rescattering strength is sampled in regions where the correlated spectral function is smaller than from the direct process. The nice agreement between the total theoretical cross section and the experiment confirms that in parallel kinematics the contribution of FSI becomes relevant only at large missing energy and it is dominated by (e,e′pπ) events.

In perpendicular kinematics the rescattering contribution is much larger, at p_m= 600 MeV/c by about 50 % as compared to the direct process. But the experimental data exceed this by an order of magnitude. Similar behaviour was observed in previous experiments and up to now the mechanism responsible for it is not understood. A possible ansatz would be the inclusion of MEC that involve the excitation of a Δ and higher resonances; these are known to be sensitive to transverse degrees of freedom.

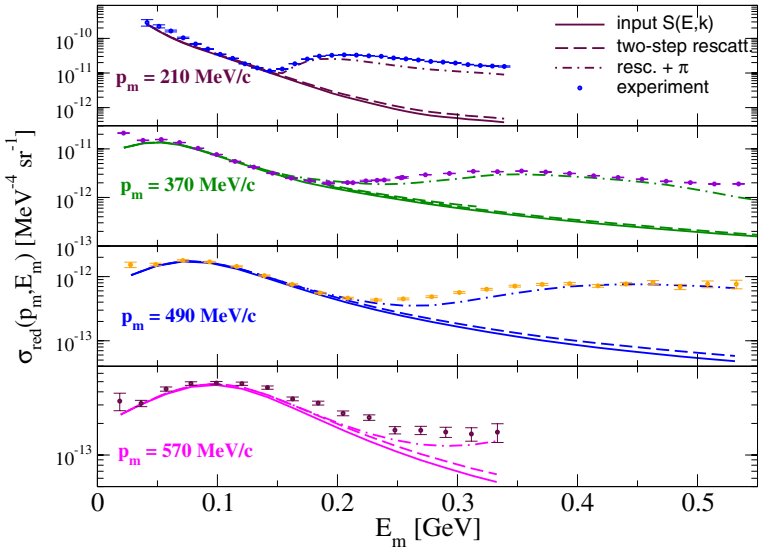

Figure **3.** Contribution from rescattering and pion production to the spectral function extracted from ^{12}C(e,e′p).

5 Results at High E_m and p_m

To obtain the spectral function from Eq. 3 a transparency factor of 0.6 was used for ^{12}C. The region of the onset of the Δ resonance is clearly visible in the data and its contribution is reduced by a cut (see also Figure 3). The results presented here are restricted to the data measured in parallel kinematics to keep the corrections on the distorted spectral function small. The experimental spectral function measured for ^{12}C is shown in Figure 4 left together with the theoretical result obtained in the SCGF approach for nuclear matter at a density comparable to ^{12}C [4]. At low momentum, around the Fermi momentum, good agreement is observed. Interestingly this is also the case for the spectral functions of refs. [3,23]. At higher p_m, however, there are significant differences as can be seen in Figure 4 on the right. The spectral function from CBF theory has its maximum at around $p_m^2/(2M)$ which reflects the impact of SRC in the quasiparticle picture valid in nuclear matter. However, the data show more strength at lower E_m and the maximum of the spectral function is shifted to smaller E_m values. This might be due to LRC in finite nuclei which are not treated in the nuclear matter calculation. Tensor correlations, which are known to be more important than central short range correlations, might also lead to a relocation of strength. Comparison of the two Green's function approaches shows a remarkable improvement of the self-consistent treatment compared to the one which contains only second order diagrams. This indicate that higher order diagrams are important and more complicated configurations than a simple hard interaction between two nucleons are involved. The spectral function from the second order Green's function approach show an increase for $E_m < 40$ MeV. This is due to the treatment of

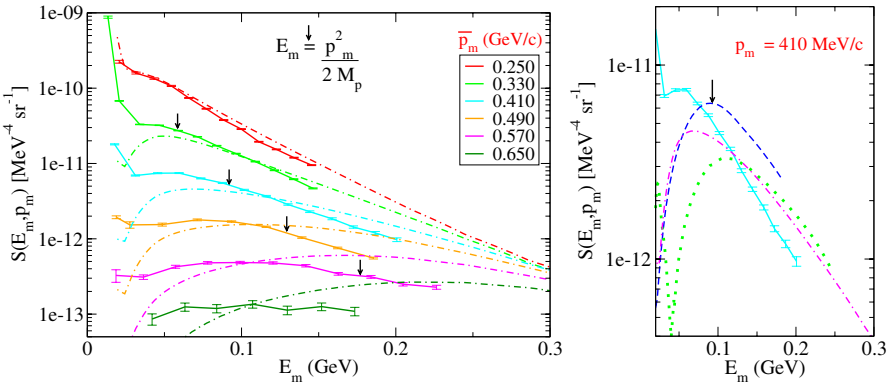

Figure **4.** Left: Spectral function for the ^{12}C nucleus. Experimental result for several momenta above the Fermi momentum are shown as solid lines with error bars. The dashed-dotted lines represent the SCGF nuclear matter spectral function at a density of $\rho = 0.08\,\mathrm{fm}^{-3}$ [4, 22]. Right: A comparison between the experimental result at $k = 410$ MeV/c (solid lines with error bars), the theoretical spectral functions by Benhar *et. al.* [23] (dashed line), the SCGF result (dashed-dotted line) and the second order Green's function approach [3] (dotted).

LRC in this calculation. On the other hand the sharp unphysical dip clearly indicates that strength is missing.

From the spectral function the momentum distribution and the number of protons found in the (E_m, p_m) region covered by the experiment can be obtained by integration. The lower integration limit is set to E_m = 40 MeV to avoid contributions from the single-particle region and LRC contributions; the upper limit is adjusted in such a way to exclude the Δ resonance. The same cuts are employed for theory. In Figure 5 the experimental momentum distribution is compared to the three theories. The result from the SCGF approach agrees best with the data whereas the other two calculations slightly over- or undershoot the data. However, one should not forget that due to the choice of the integration limits in E_m the comparison depends somewhat on the different shapes of the experimental and theoretical spectral functions.

Integrating the spectral function over the (E_m,p_m) region covered by the experiment (p_m = 0.23 - 0.67 GeV/c) and using the integration limits discussed above, one obtains the correlated strength. This strength, 10 % of the total strength, represents the number of protons which are located outside the IPSM region and appears in the

Table **1.** Correlated strength (quoted in terms of the number of protons in ^{12}C).

Experiment	0.61 $\pm$0.06
Greens function theory [3]	0.46
CBF theory [2]	0.64
SCGF theory [4]	0.61

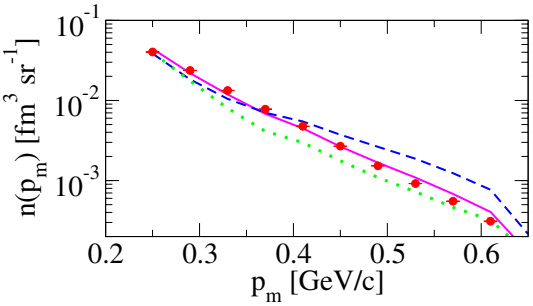

Figure **5.** Momentum distribution of the data (circles) compared to the theory of refs. [3] (dots), [4] (solid) and [23] (dashed). The lower integration limit is chosen as 40 MeV, the upper one to exclude the Δ resonance.

region covered by the experimental setup. The numbers obtained from the data and from three theories are quoted in Table 1. To account for FSI a correction of –4 % has to applied to the experimental value in Table 1 [6, 10]. Good agreement is found between data and the CBF theory as well as with the SCGF approach.

Comparison of the results to the ones obtained for heavier nuclei (Al, Fe, Au) shows that the shape of the spectral function for C, Al, and Fe ist quite similar. For Au a larger contribution from the broader resonance region is obvious and the maximum of the spectral function is shifted to higher E_m. The correlated strength for Al, Fe and Au is 1.05, 1.12 and 1.7 times the strength for C normalized to the same number of protons. This increase cannot be solely explained by rescattering (about 10 % increase for Au) but MEC's have probably taken into account. On the other hand MEC's are related to short-range N-N pairs and therefore should not show a large dependence on the size of the nucleus. Another contribution may be coming from the stronger tensor correlations in asymmetric nuclear matter [24, 25]. For Au an increase of the 20 – 30 % of the proton spectral function is expected compared to the symmetric case (^{12}C) [26]. This still cannot explain the entire increase of the spectral strength from ^{12}C to Au.

Acknowledgments

This work was supported by the Schweizerische Nationalfonds (SNF), the US Dept. of Energy and the US National Science Foundation.

References

1. P. K. A. deWitt Huberts, *J. Phys. G* **16**, 507 (1990).
2. O. Benhar, A. Fabrocini, and S. Fantoni, *Nucl. Phys. A* **505**, 267 (1989).
3. H. Műther, G. Knehr, and A. Polls, *Phys. Rev. C* **52**, 2955 (1995).
4. T. Frick and H. Müther, *Phys. Rev. C* **68**, 034310 (2003).

5. D. Rohe, *Habilitationsschrift*, Universität Basel (2004).
6. C. Barbieri, *Proc. Nuint workshop* Okayama, to be published in *Nucl. Phys. B Suppl.* (2006).
7. C. Barbieri, D. Rohe, I. Sick, and L. Lapikás, *Phys. Lett. B* **608**, 47 (2005).
8. T. de Forest, *Nucl. Phys. A* **392**, 232 (1983).
9. D. Rohe, O. Benhar *et al.*, *Phys. Rev. C* **72**, 054602 (2005).
10. C. Barbieri and L. Lapikás, *Phys. Rev. C* **70**, 054612 (2004).
11. T. G. O′Neill *et al.*, *Phys. Lett. B* **351**, 87 (1995).
12. D. Abbott *et al.*, *Phys. Rev. Lett.* **80**, 5072 (1998).
13. K. Garrow *et al.*, *Phys. Rev. C* **66**, 044613 (2002).
14. G. Garino *et al. Phys. Rev. C* **45**, 780 (1992).
15. O. Benhar, A. Fabrocini, S. Fantoni, and I. Sick, *Nucl. Phys. A* **579**, 493 (1994).
16. J. Mougey *et al.*, *Nucl. Phys. A* **262**, 461 (1976).
17. I. Sick, *private communication* (1993).
18. J. W. Van Orden, W. Truex, and M.K. Banerjee, *Phys. Rev. C* **21**, 2628 (1980).
19. O. Benhar, A. Fabrocini, and S. Fantoni, *Phys. Rev. C* **41**, R24 (1990).
20. H. Müther and I. Sick, *Phys. Rev. C* **70**, 041301(R) (2004).
21. D. Rohe *et al.*, *Phys. Rev. Lett.* **93**, 182501 (2004).
22. T. Frick, Kh. S. A. Hassaneen, D. Rohe, and H. Müther, *Phys. Rev. C* **70**, 024309 (2004).
23. O. Benhar, A. Fabrocini, S. Fantoni, and I. Sick, *Nucl. Phys. A* **579**, 493 (1994).
24. P. Konrad, H. Lenske, and U. Mosel, *Nucl. Phys. A* **756**, 192 (2004).
25. Kh. S. A. Hassaneen and H. Müther, *Phys. Rev. C* **70**, 054308 (2004).
26. H. Műther, *private communication* (2004).